ChemPubSoc Europe

DOI: 10.1002/ejoc.201700861

EurJOC European Journal of Organic Chemistry
Communication

Corannulenes

Decakis(arylthio)corannulenes: Transferable Photochemical and Redox Parameters and Photovoltaic Device Performance

Yanan Deng,[a] Bokai Xu,[a] Edison Castro,[b] Olivia Fernandez-Delgado,[b] Luis Echegoyen,[b] Kim K Baldridge*[a] and Jay S. Siegel*[a]

Abstract: Absorption and redox properties of seven decakis(phenylthio)corannulene derivatives **3a**–**3g** lead to a model for estimating material properties in persulfurated aromatic compounds. The same series is evaluated for performance in bulk heterojunction and perovskite photovoltaic devices.

Introduction

Corannulene (**1**) is a convenient starting material for the synthesis of a breadth of curved aromatic materials.[1,2] Phenylthio substituents attached to aromatic cores result in a reduction of the HOMO–LUMO gap by decreasing the ionization potential (raising HOMO) and increasing the electron affinity (lowering LUMO).[3] This substituent effect facilitates n-type and p-type electron transport concomitantly. In the case of **1**, which can bear ten such substituents, the longest-wavelength UV/Vis absorption changes from about 290 nm in **1** to 420 nm in decakis(phenylthio)corannulene **3g**, a change in the optical gap of 130 nm.[4] Electrochemically, the redox gap from first oxidation to first reduction potential is 3.6 eV for **1**[5] vs. 2.0 eV for **3g**,[4] a change in redox gap of 1.6 eV. Focusing just on the reduction potential of **1** and **3g**, which relates to the electron affinity, the change is nearly 1.0 eV (–2.45 eV vs. –1.5 eV, respectively). Peripheral substitution on the phenyl rings of **3g** raises some questions: Can such a remote substituent exert a materially meaningful influence (e.g., Δ 0.2 eV or > Δ 20 nm) worth the synthetic effort? If so, what is the mechanism of HOMO/LUMO perturbation? Can transferable substituent parameters be established to predict the properties of similarly substituted polynuclear aromatic hydrocarbons (PAHs) generally? Can these properties be correlated with materials performance, for example in a photovoltaic device? Synthesis of a set of seven derivatives of **3** and measurement of their absorption spectra and reduction potentials directly addresses these questions.

Results and Discussion

Perchlorination of **1** by BMC conditions,[6] affords tetradecachlorocorannulene that can be rearomatized by refluxing in diphenyl ether to give decachlorocorannulene **2**.[7] Synthesis of **3g** uses **2** and thiophenoxide with sodium hydride as base in a polar solvent such as dimethylimidazolone (DMI) at 60 °C for 24 h.[4,7a] This general method, by varying the thiophenoxide, readily allowed the preparation of the series **3a**–**f** (**3e** in *ortho*-dichlorobenzene at 160 °C). The substituents were kept to chloro and methyl groups placed in the *meta* or *para* positions, in an attempt to produce a roughly isochoric cognate series (Scheme 1).

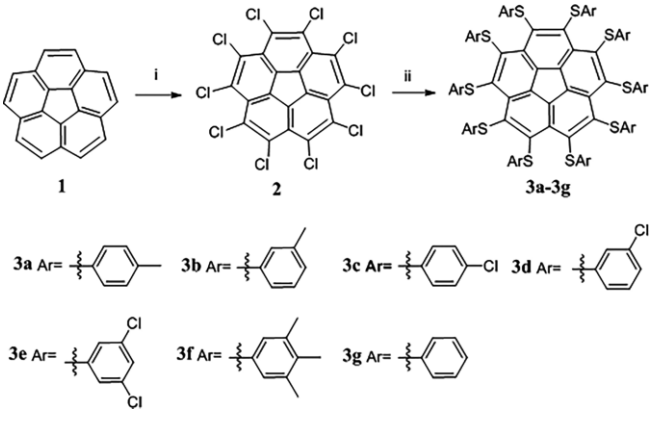

Scheme 1. *Reaction conditions:* (i) 1) $SOCl_2$, $AlCl_3$, S_2Cl_2; 2) Ph_2O, 180 °C, 24 h. Total yield: 57 %. (ii) For **3e**: 1) NaH, ArSH, dry *ortho*-dichlorobenzene, room temp., N_2, 10 min; 2) compound **2**, from room temp. to 160 °C, N_2, 24 h; yield: 91 %. For other products: 1) NaH, ArSH, dry DMI, room temp., N_2, 10 min; 2) compound **2**, from room temp. to 60 °C, N_2, 24 h. yield: **3a** 75 %, **3b** 46 %, **3c** 35 %, **3d** 14 %, **3f** 62 %, **3g** 50 %. DMI: 1,3-dimethyl-2-imidazolidinone; NaH: sodium hydride.

Comparison of the crystal structure of **3a** with that of **3g**[8] reveals that the general size, shape, and specific conformation of the two molecules are similar (Figure 1). The molecular packing in the two crystals retains the same layered structure; the bowl carbons and sulfur atoms define in a rough stratum, which is separated by the phenyl fingers pointing alternately up/down around the ring. This alignment could be favorable for electron transport.

[a] *School of Pharmaceutical Science and Technology, Tianjin University, 92 Weijin Road, Nankai District, Tianjin 300072, China*
E-mail: dean_spst@tju.edu.cn
http://health.tju.edu.cn/
[b] *Department of Chemistry, University of Texas at El Paso, 500 West University Avenue, El Paso, <countrypart/>TX 79968, USA*
Supporting information and ORCID(s) from the author(s) for this article are available on the WWW under https://doi.org/10.1002/ejoc.201700861.

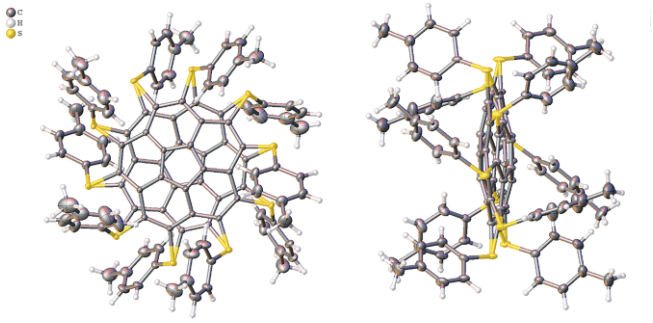

Figure 1. Overlapping orientations in the **s**ingle crystal of **3a**: left: face view; right: side view. Solvents of crystallization excluded for clarity.

The first reduction potential measurements (Table 1; Figure 2) across the series show great variability (–1.0 to –1.7 eV). Arranging the data in an order consistent with the sum of the standard Hammett values[9] (σ_m and σ_p) reveals a trend in which more electron-withdrawing character correlates with the compound with better electron-acceptor capability, and more electron-donating character with the compound being a worse electron acceptor.

Table 1. Summary of electrochemical data.

Pro	σ	E_c[a] [V]	$E_{1/2}$ [V]	$E_a - E_c$ [mV]	Ip_a/Ip_c	pK_a (SH)
3e	0.74	–1.05 [-1.13][b]	0.94	215	0.85	5.07
3d	0.37	–1.13	1.17	264	0.89	5.83
3c	0.23	–1.47 [-1.40][b]	1.25	430	0.93[c]	6.12
3g	0	–1.49 [-1.56][b]	1.41	171	1.01	6.61
3b	–0.07	–1.58	1.46	237	1.09	6.70
3a	–0.17	–1.63	1.51	243	1.20	6.81
3f	–0.31	–1.67 [-1.70][b]	1.57	205	0.92	7.03

[a] Cyclic voltammetry: 1 mM in 0.07 M $TBAPF_6$/THF solution at 298 K. Electrodes: Glassy carbon working electrode; reference electrode Ag/Ag^+ in ACN; platinum wire counter electrode. Scan rate = 0.1 V/s. The internal standard was the ferrocinium/ferrocene couple standard potential (+0.085 V for THF). [b] [Bracketed] values are B97D/Def2-TZVPP(THF) $E° = \Delta E/nF$, where n = 1, F = 1 eV, referenced to Ag/AgCl. [c] Measured at 0.01 V/s.

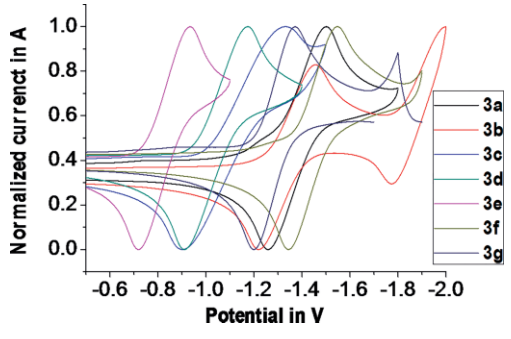

Figure 2. Cyclic voltammograms for **3a**–**3g**. Note, the small wave in **3g** at ca. –0.85 V is due to a persistent minor impurity after purification.

Originally, Hammett values were derived from pK_a studies on benzoic acid in water and ascribed to effects of the substituent's ability to influence carboxylate and carboxylic acid states across a benzene ring.[10] In the present series, one might hypothesize that the relative energies of the protonated (i.e. neutral) and unprotonated (i.e. anionic) state of the thiophenols might correlate better with the first reduction potentials of **3a**–**3g**, especially if the electronic character of the sulfur atoms play a determinant role. Indeed, a plot of the pK_a of the corresponding thiophenol vs. the half reduction potential for the series **3a**–**g** reveals a much stronger correlation (R^2 = 0.996; Figure 3); thus, prompting a working model in which the electronic properties of the persulfurated aromatic core can be tuned remotely through the periphery of the molecule. With ten substituents, even subtle single-substituent effects can manifest substantial changes in the redox properties of the compound.

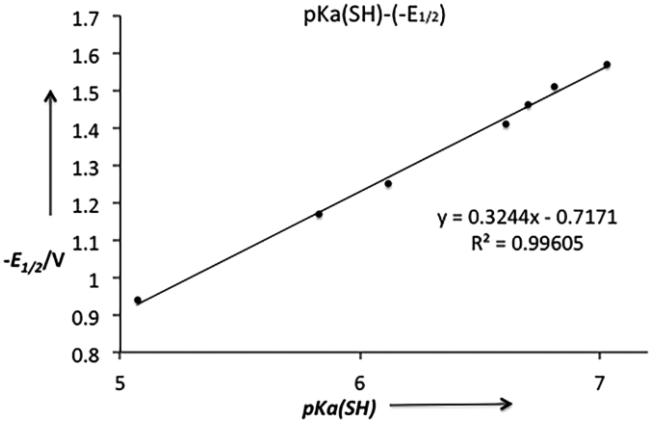

Figure 3. Correlation of pK_a(ArSH) vs. $E_{1/2}$.

The variability across the long-wavelength UV/Vis data is much less and does not track with the simple inference that lower a LUMO leads to longer-wavelength absorption (Figure 4). In contrast, the compounds bearing substituents of greater electron-donating character correlate with longer-wavelength absorption and those with greater electron-withdrawing character correlate with shorter-wavelength absorption. This result is consistent with the electron-donating substituents raising both HOMO and LUMO levels, but raising HOMO even more; electron-withdrawing substituents lowering both HOMO and LUMO levels, but lowering HOMO even more. Thus, electron-donating substituents should cause a narrowing of the HOMO–LUMO gap, and electron-withdrawing substituents should

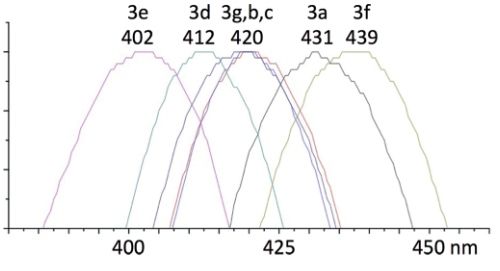

Figure 4. Normalized experimental UV/Vis absorption in THF. Epsilon values x10^4: **3a**: 1.18, **3b**: 1.27, **3c**: 1.44, **3d**: 1.16, **3e**: 1.06, **3f**: 1.28, **3g**: 1.25.

cause a widening of the HOMO–LUMO gap. TD-DFT wB97xD/Def2-TZVPP//B97-D/Def2-TZVPP(THF) calculated UV spectra support a longer wavelength absorption of **3f** compared to **3g**, but show little difference between **3e** and **3g** (Figure 5).

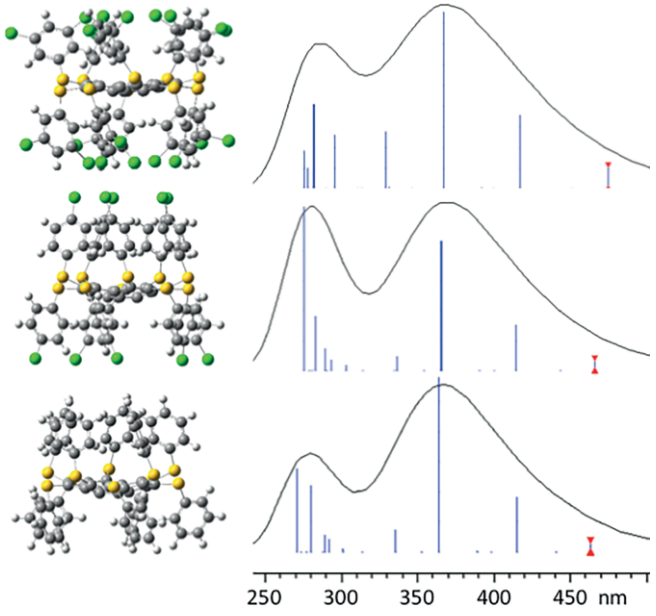

Figure 5. TD-DFT wB97xD/Def2-TZVPP//B97-D/Def2-TZVPP(THF) calculated UV spectra for **3e**, **3g**, and **3f**.

By measuring the corresponding oxidation potentials for **3e**, **3f**, and **3g**, the redox gap (first oxidation to first reduction potential) was derived. Referencing to **3g**, when electron-withdrawing chlorine groups are added, as in **3e**, the HOMO and LUMO energy are pulled down, whereas when electron-donating methyl groups are added, as in **3f**, the HOMO and LUMO energy are pushed up (Figure 6). Additionally, from the longest-wavelength maximum absorption, one infers that the optical gap of **3e** is largest, followed by **3g**, and then **3f** (cf. Figure 4).

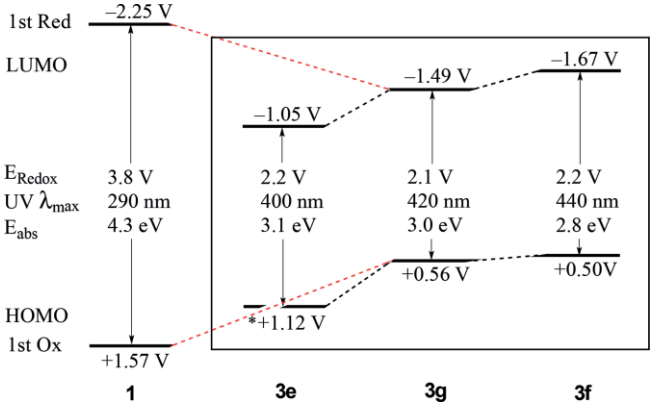

Figure 6. HOMO–LUMO trends gauged from UV spectra and voltammetry.

Assuming a model with additive substituent effects and transferable substituent parameters, the redox properties of similar aromatic systems, such as dodecakis-X-coronene,[11] octakis-X-pyrene,[12] and dodecakis-X-perylene[13] can be predicted (Table 2). The change in redox potential can be deduced by multiplying the number of substitution sites of each compound by the value of a specific substituent effect derived from decakis-X-corannulene. Presumably this could also be applied to the prediction of pK_a and pK_R values for persulfurated cyclopentadienyl anions and tropylium cations.

Table 2. Redox potential predictions for selected persulfurated PAH's [V].

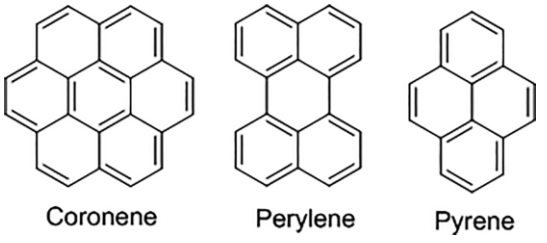

		Parent	Cl_2PhS	PhS	Me_3PhS
Coronene	red	−2.02[a]	−0.58	−1.11	−1.32
	ox	1.38[a]	0.84	0.17	0.10
	red	−2.13[b]	−0.69	−1.22	−1.43
	ox	1.40[b]	0.86	0.19	0.12
Perylene	red	–	–	–	–
	ox	0.54[b]	0	−0.67	−0.74
Pyrene	red	−2.2[a]	−1.0	−1.44	−1.62
	ox	1.33[a]	0.88	0.32	0.26

[a] Electrodes: Glassy carbon working electrode; a saturated calomel electrode as reference electrode; platinum wire counter electrode.[11b,12] [b] Electrodes: Glassy carbon working electrode; an Ag/AgCl electrode as reference electrode; platinum wire counter electrode.[11a,13]

Independent of this study, perthiophenylcoronene has been synthesized and characterized electrochemically.[14] The measured first reduction potential is −1.02 V and corroborates with the value predicted by application of the transferable substituent parameter (−1.11 V).

The tunable series of perthioarylcorannulenes allows one to test an additional hypothesis about a possible correlation of the reduction potential with photovoltaic device performance. Specifically, two different types of photovoltaic devices were contemplated: bulk heterojunction and perovskite.

Bulk Heterojunction (BHJ) Solar Cells

In order to evaluate the photovoltaic properties of **3a**–**3g**, organic solar cells were fabricated using a device architecture of ITO/PEDOT:PSS/P3HT:**XX**/Al, where ITO is indium tin oxide, PEDOT is poly(3,4-ethylenedioxythiophene), PSS is poly(styrenesulfonate), P3HT is poly (3-hexylthiophene), and **XX** = phenyl-C_{60}- butyric acid methyl ester, $PC_{61}BM$, or **3a**–**3g**.

For these cells, 1/1 donor:acceptor mass blend ratios were tested. The active layer was deposited by spin-coating a chlorobenzene solution (20 mg/mL) followed by thermal annealing at 150 °C for 10 min. The current density-voltage (*J*–*V*) curves of the devices are shown in Figure 7. Compound **3a** showed the best performance, with a V_{oc} = 0.42 V, J_{sc} = 5.35 mA/cm^2, *FF* = 0.55, and PCE = 1.23 %. The device parameters are summarized in Table 3.

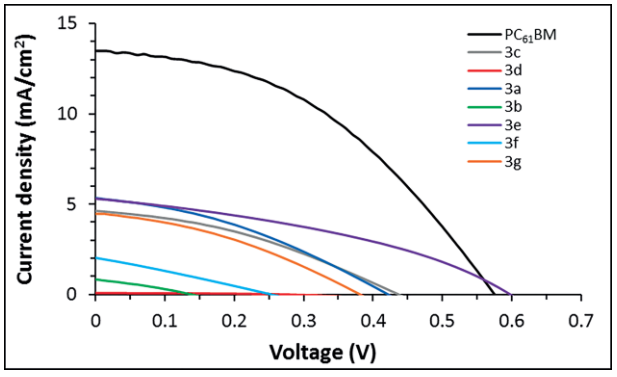

Figure 7. *J–V* curves of BHJ organic solar cells based on **3a**–**3g** with $PC_{61}BM$ used as the control.

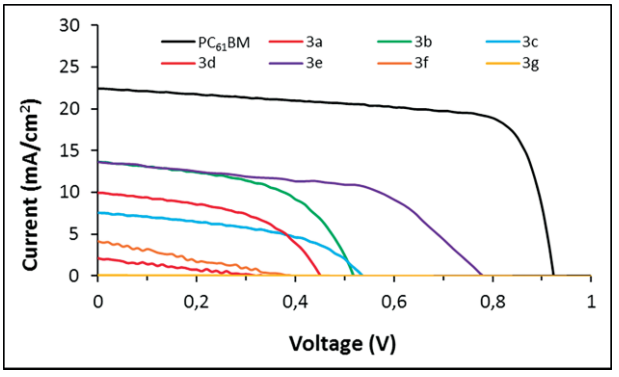

Figure 8. *J–V* curves of PSCs based on corannulenes **3a**–**3g** as the ETMs; $PC_{61}BM$ was used as control.

Table 3. Summary of device parameters for P3HT: **3a**–**3g** solar cells, under an AM1.5G illumination at 100 mW/cm².

Comp.	J_{sc} [mA/cm²]	V_{oc} [V]	FF	PCE [%] ± SE
$PC_{61}BM$	13.46	0.57	0.43	3.17 ± 0.05 (3.32)
3a	5.35	0.42	0.55	0.92 ± 0.08 (1.23)
3b	0.82	0.18	0.31	0.03 ± 0.01 (0.05)
3c	4.62	0.44	0.36	0.59 ± 0.04 (0.73)
3d	0.07	0.26	0.38	0.01 ± 0.00 (0.01)
3e	5.28	0.60	0.37	0.95 ± 0.06 (1.18)
3f	2.01	0.25	0.27	0.09 ± 0.01 (0.14)
3g	4.50	0.12	0.42	0.20 ± 0.01 (0.23)

[a] PCEs are average values for eight devices with four cells each. The values in parentheses are the maximum PCEs. SE is the standard error.

Perovskite Solar Cells (PSCs)

To investigate the selective electron-transporting properties of **3a**–**3g**, planar structure devices with a configuration of ITO/PEDOT:PSS/$CH_3NH_3PbI_3$/**XX**/Al (**XX** = $PC_{61}BM$ or **3a**–**3g**) were fabricated. In this configuration, PEDOT:PSS is used as the hole-transport material (HTM). As far as we know, this is the first reported use of functionalized corannulene as an electron-transport material (ETM) in inverted PSCs. The most common and efficient ETMs reported are fullerenes and their derivatives.[15]

The perovskite layer of the device was prepared by spin-coating a $CH_3NH_3PbI_3$ (1 M in DMF) solution onto a PEDOT:PSS layer. After annealing at 75 °C for 60 min, $PC_{61}BM$ or **3a**–**3g** (20 mg/mL in chlorobenzene) were spin-coated on the perovskite substrates. Finally, Al was thermally evaporated under a pressure of 2×10^{-6} Torr through a shadow mask. The thickness of each layer was measured by using a profilometer, showing that the PEDOT:PSS, perovskite, and $PC_{61}BM$ or **3a**–**3g** layers had a thickness of approximately 40 nm, 350 nm, and 60 nm, respectively.

The most efficient device, using **3e** as ETM, yielded a maximum PCE of 7.91 %. Devices based on $PC_{61}BM$ as ETM yielded a maximum PCE of 15.05 % under the same conditions. The *J–V* curves of the devices are shown in Figure 8 and the photovoltaic performance parameters V_{oc}, J_{sc}, *FF*, and PCE are summarized in Table 4.

Table 4. Summary of device parameters of P3HT:corannulenes (**3a–3g**) solar cells, under the illumination of AM1.5G, 100 mW/cm².

Comp.	J_{sc} [mA/cm²]	V_{oc} [V]	FF	PCE [%] ± SE
$PC_{61}BM$	22.38	0.92	0.73	14.71 ± 0.18 (15.05)
3a	0.09	0.44	0.25	0.00
3b	14.86	0.46	0.45	2.8 ± 0.08 (3.07)
3c	8.33	0.54	0.48	1.85 ± 0.09 (2.16)
3d	11.20	0.42	0.37	1.54 ± 0.07 (1.74)
3e	14.50	0.78	0.45	6.82 ± 0.30 (7.91)
3f	0.02	0.33	0.27	0.00
3g	0.04	0.49	0.20	0.00

[a] PCEs are average values for eight devices with four cells each. The values in parentheses are the maximum PCEs. SE is the standard error.

Conclusion

In conclusion, a set of seven decakis(phenylthio)corannulene derivatives **3a**–**g** has been synthesized. A slight modification of the synthetic method was made to obtain the desired product **3e**. Analysis of cyclic voltammograms, UV/Vis spectra, and other parameters provided a model for substituent tuning of the HOMO–LUMO levels across the series. The HOMO/LUMO levels for **3a**–**3g** fall in a comparable range with standard photovoltaic-cell components (Figure 9), which suggested that **3a**–**g** could be alternative materials for $PC_{61}BM$ in photovoltaic cells and related devices. In bulk heterojunction and perovskite solar cells, **3e** showed the highest efficiency (**3e** ≈ **3a** for BHJs) and the lowest solution reduction potential; however, a general correlation of reduction potential and efficiency was not established.

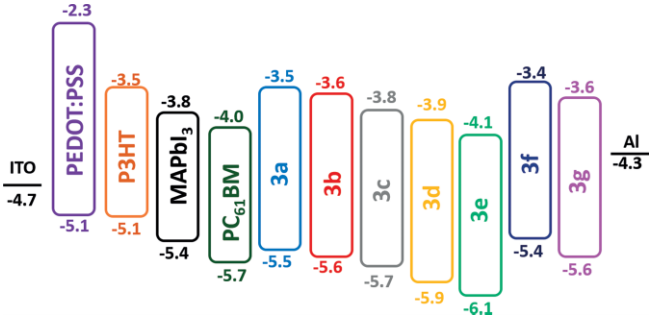

Figure 9. Energy level diagram of bulk heterojunction and perovskite solar cells to compare the new corannulene **3a**–**3g** against standardly used cells.

CCDC 1557751 (for **3a**) contains the supplementary crystallographic data for this paper. These data can be obtained free of charge from The Cambridge Crystallographic Data Centre.

Acknowledgments

J. S. S., K. K. B., Y. D., and B. X. thank the National Basic Research Program of China (2015CB856500) and the Synergetic Innovation Center of Chemical Science and Engineering (Tianjin) for support of this work. J. S. S. and K. K. B thank the Qian Ren Scholar Program of China. L. E. thanks the US National Science Foundation (NSF) for generous support of this work under the NSF-PREM program (DMR 1205302) and the CHE-1408865. The Robert A. Welch Foundation is also gratefully acknowledged for an endowed chair to L. E. (Grant AH-0033). Jun Xu is acknowledged for assistance with crystallographic details.

Keywords: Corannulenes · Photophysics · Cyclic voltammetry · Molecular electronics · Solar cells

[1] Y.-T. Wu, J. S. Siegel, *Chem. Rev.* **2006**, *106*, 4843.
[2] A. M. Butterfield, B. Gilomen, J. S. Siegel, *Org. Process Res. Dev.* **2012**, *16*, 664.
[3] a) M. Gingras, J.-M. Raimundo, Y. M. Chabre, *Angew. Chem. Int. Ed.* **2006**, *45*, 1686; *Angew. Chem.* **2006**, *118*, 1718; b) M. Mayor, J.-M. Lehn, *J. Am. Chem. Soc.* **1999**, *121*, 11231; c) M. Mayor, J.-M. Lehn, K. M. Fromm, D. Fenske, *Angew. Chem. Int. Ed. Engl.* **1997**, *36*, 2370; *Angew. Chem.* **1997**, *109*, 2468.
[4] A. Steinauer, A. M. Butterfield, A. Linden, A. M. Ontario, D. C. Buck, R. W. Cotta, L. Echegoyan, K. K. Baldridge, J. S. Siegel, *J. Braz. Chem. Soc.* **2016**, *27*, 1866.
[5] T. J. Seiders, K. K. Baldridge, R. Gleiter, J. S. Siegel, *Tetrahedron Lett.* **2000**, *41*, 4519.
[6] a) M. Ballester, C. Molinet, J. Castañer, *J. Am. Chem. Soc.* **1960**, *82*, 4254; b) M. Ballester, J. R. Figueras, J. Castaner, *J. Am. Chem. Soc.* **1971**, *93*, 2215.
[7] a) P. C. Cheng, Boston College **1996**; b) T. J. Seiders, E. L. Elliott, G. H. Grube, J. S. Siegel, *J. Am. Chem. Soc.* **1999**, *121*, 7804; c) A. M. Butterfield, University of Zürich (Zürich), **2008**.
[8] K. K. Baldridge, K. I. Hardcastle, T. J. Seiders, J. S. Siegel, *Org. Biomol. Chem.* **2010**, *8*, 53.
[9] a) C. Hansch, A. Leo, R. W. Taft, *Chem. Rev.* **1991**, *91*, 165; b) J. Shorter, *Pure Appl. Chem.* **1994**, *66*, 2451; c) J. Shorter, *Aust. J. Chem.* **1998**, *51*, 525.
[10] L. P. Hammett, *J. Am. Chem. Soc.* **1937**, *59*, 96.
[11] a) O. Kataeva, M. Khrizanforov, Y. Budnikova, D. Islamov, T. Burganov, A. Vandyukov, K. Lyssenko, B. Mahns, M. Nohr, S. Hampel, M. Knupfer, *Cryst. Growth Des.* **2016**, *16*, 331; b) S. Hirayama, H. Sakai, Y. Araki, M. Tanaka, M. Imakawa, T. Wada, T. Takenobu, T. Hasobe, *Chem. Eur. J.* **2014**, *20*, 9081.
[12] M. A. Tehfe, J. Laleve, M. S. Fabrice, B. Graff, N. Blanchard, J. P. Fouassier, *Macromolecules* **2012**, *45*, 1746.
[13] J. D. Wood, J. L. Jellison, A. D. Finke, L. C. Wang, K. N. Plunkett, *J. Am. Chem. Soc.* **2012**, *134*, 15783.
[14] J. H. R. Tucker, M. Gingras, H. Brand, J.-M. Lehn, *J. Chem. Soc. Perkin Trans. 2* **1997**, 1303.
[15] J. Liu, G. Wang, K. Luo, X. He, Q. Ye, C. Liao, J. Mei, *ChemPhysChem* **2017**, *18*, 617.

Received: June 17, 2017

